Published OnlineFirst June 26, 2018; DOI: 10.1158/0008-5472.CAN-18-0267

Tumor Biology and Immunology

Cancer Research

Cotargeting Ephrin Receptor Tyrosine Kinases A2 and A3 in Cancer Stem Cells Reduces Growth of Recurrent Glioblastoma

Maleeha A. Qazi[1], Parvez Vora[1], Chitra Venugopal[1], Jarrett Adams[2], Mohini Singh[1], Amy Hu[2], Maryna Gorelik[2], Minomi K. Subapanditha[1], Neil Savage[1], Jiahe Yang[2], Chirayu Chokshi[1], Max London[2], Alexander Gont[3], David Bobrowski[1], Natalie Grinshtein[3], Kevin R. Brown[2], Naresh K. Murty[4], Johan Nilvebrant[2], David Kaplan[3], Jason Moffat[2], Sachdev Sidhu[2], and Sheila K. Singh[1,4]

Abstract

Glioblastoma (GBM) carries a dismal prognosis and inevitably relapses despite aggressive therapy. Many members of the Eph receptor tyrosine kinase (EphR) family are expressed by GBM stem cells (GSC), which have been implicated in resistance to GBM therapy. In this study, we identify several EphRs that mark a therapeutically targetable GSC population in treatment-refractory, recurrent GBM (rGBM). Using a highly specific EphR antibody panel and CyTOF (cytometry by time-of-flight), we characterized the expression of all 14 EphR in primary and recurrent patient-derived GSCs to identify putative rGBM-specific EphR. EPHA2 and EPHA3 coexpression marked a highly tumorigenic cell population in rGBM that was enriched in GSC marker expression. Knockdown of EPHA2 and EPHA3 together led to increased expression of differentiation marker GFAP and blocked clonogenic and tumorigenic potential, promoting significantly higher survival *in vivo*. Treatment of rGBM with a bispecific antibody against EPHA2/A3 reduced clonogenicity *in vitro* and tumorigenic potential of xenografted recurrent GBM *in vivo* via downregulation of AKT and ERK and increased cellular differentiation. In conclusion, we show that EPHA2 and EPHA3 together mark a GSC population in rGBM and that strategic cotargeting of EPHA2 and EPHA3 presents a novel and rational therapeutic approach for rGBM.

Significance: Treatment of rGBM with a novel bispecific antibody against EPHA2 and EPHA3 reduces tumor burden, paving the way for the development of therapeutic approaches against biologically relevant targets in rGBM. *Cancer Res; 78(17); 5023–37. ©2018 AACR.*

Introduction

Glioblastoma (GBM) is the most malignant primary brain tumor in adults (1, 2). Despite aggressive standard therapy consisting of surgical resection followed by radiation and chemotherapy, tumor regrowth and patient relapse remain inevitable. On average, patients face disease relapse at 7–9 months post-diagnosis and succumb to disease progression with a median survival of only 15 months (3, 4). The dismal prognosis of GBM has been increasingly attributed to extensive genetic, epigenetic, cellular, and functional heterogeneity (5–9), allowing for redundancy in signaling pathways and rendering single-agent therapy obsolete for long-term disease remission and cure. Moreover, the genomic landscape of recurrent GBM has been shown to diverge significantly from the primary GBM, as actionable targets identified in primary, treatment-naïve GBM are not present at recurrence. Rather, recurrent disease is instead driven by a different mutational and signaling profile (10–12). There is also accumulating evidence suggesting that GBMs may be instigated by stem cell–like populations termed GBM stem cells (GSC; refs. 13–16). Moreover, GSCs are thought to account for GBM recurrence after therapy as cells with GSC properties are resistant to radiation and chemotherapeutic agents (17–20). Together, this evidence implies that treatment of recurrent GBM should be informed by the identification of molecular targets specific to its evolved molecular landscape, and a poly-targeting approach could better address the advanced clonal heterogeneity that generates cellular escape from therapy, resulting in treatment resistance.

The EphR tyrosine kinase family, with 14 members, coordinates cell positioning, tissue, and organ patterning during development, and is expressed in most adult stem cell niches and many cancers (21–23). Various members of the EPHA/EPHRIN-A and EPHB/EPHRIN-B subfamilies have been shown to play a role in GBM cell migration, invasion, and angiogenesis (24–27). The expression of EPHA2, EPHA3, EPHA4, EPHA7, and EPHB2 correlates with poor patient outcome in GBM, and each has a distinct role in GBM tumorigenicity, invasiveness, or maintenance of the GSC pool. In particular, EPHA2 has been shown to drive tumorigenicity in GSCs, and infusion of EPHRINA1-Fc into intracranial xenografts elicited strong tumor-suppressing effects (24). EPHA2 overexpression has also been shown to promote invasiveness

[1]Stem Cell and Cancer Research Institute, McMaster University, Hamilton, Ontario Canada. [2]The Donnelly Centre, University of Toronto, Toronto, Ontario, Canada. [3]The Hospital for Sick Children, Toronto, Ontario, Canada. [4]Department of Surgery, McMaster University, Hamilton, Ontario, Canada.

Note: Supplementary data for this article are available at Cancer Research Online (http://cancerres.aacrjournals.org/).

Corresponding Author: Sheila K. Singh, McMaster Stem Cell and Cancer Research Institute, MDCL 5027, Michael DeGroote Centre for Learning and Discovery, 1280 Main Street West, Hamilton, Ontario L8S 4K1, Canada. Phone: 905-521-2100, ext. 75237; Fax: 905-521-9992; E-mail: ssingh@mcmaster.ca

doi: 10.1158/0008-5472.CAN-18-0267

Published OnlineFirst June 26, 2018; DOI: 10.1158/0008-5472.CAN-18-0267

of GSCs *in vivo* in cooperation with the AKT signaling pathway (27, 28). Similarly, EPHA3 has also emerged as a GSC marker, which is overexpressed in GBM and maintains GBM cells in a stem-like state (25). While these data validate EPHA2 and EPHA3 as therapeutic targets in brain tumors, the literature to date has only profiled or targeted single EphRs in treatment-naïve GBM and suggests single targeting of an EphR would leave other putative EphR-driven GSC populations to seed tumor recurrence. In addition, what have not been explored are the complex putative effects of multiple EphR family members dynamically activated or suppressed through therapy delivery and tumor progression.

In this study, we used an EphR profiler to simultaneously assess the protein expression of all EphRs in cells comprising primary and recurrent GBM, to identify the putative cooperative role of multiple EphRs in driving GBM tumorigenesis. Given the established importance of EPHA2 and EPHA3 individually in maintaining GSCs, we wanted to explore whether EPHA2 and EPHA3 together mark an even more potent tumorigenic cancer stem cell population in recurrent GBM. Considering the complex signaling pathways orchestrated by multiple EphRs, we also examined whether cotargeting of EPHA2 and EPHA3 using a bispecific antibody approach will impact the functional GSC pool more effectively than monotherapies.

Materials and Methods

Patient tumors

Human GBM brain tumors were obtained from consenting patients, as approved by the Hamilton Health Sciences/McMaster Health Sciences Research Ethics Board (REB # 07366), in compliance with Canada's Tri-Council Policy Statement on the Ethical Conduct for Research Involving Humans and the International Ethical Guidelines for Biomedical Research Involving Human Subjects. GBM4 was a kind gift from Dr. Hiroaki Wakimoto (Massachusetts General Hospital, Boston, MA). Patient demographics are presented in Supplementary Table S1.

Dissociation and culture of GBM tissue

Human GBM tissue was dissociated and cells were maintained in NeuroCult complete media (StemCell Technologies; 10 ng/mL bFGF, 20 ng/mL EGF, and 2 μg/mL heparin) either as tumorspheres or grown adherently on poly-L-ornithine/laminin-coated plates.

Eph profiler

Receptor-selective antibodies for all 14 Eph homologs were used to profile the expression of EphRs in primary and recurrent GBMs.

In vitro chemoradiotherapy

We treated primary GBM BT602 with radiation and temozolomide as described in Qazi and colleagues (20).

Flow cytometry analysis

The percentage expression of EPHA2, EPHA3, EPHRINA1, and EPHRINA5 was determined on a MoFlo XDP flow cytometer (Beckman Coulter) along with Summit 5.4 software using in-house anti-EPHA2 Fab with Alexa Fluor 488 as secondary antibody, in-house anti-EPHA3 Fab with APC as secondary antibody, in-house anti-EPHRINA1 Fab with AF488 as secondary antibody, and in-house anti-EPHRINA5 Fab with APC as secondary antibody. Data were analyzed with Kaluza Flow Analysis software.

CyTOF and viSNE analysis

Expression of EphRs along with a panel of stem cell markers implicated in GBM tumorigenesis was determined by cytometry by time-of-flight (CyTOF). Lanthanide metal tags were selected using Fluidigm Maxpar Panel Designer and conjugated to commercial IgGs using Fluidigm MAXPAR X8 antibody labeling kit following manufacturer's instructions (Fluidigm). In brief, commercial IgGs targeting MAP2 (^{153}Eu; Thermo Fisher Scientific, 13–1500), CD133 (^{164}Dy; Miltenyi Biotec, 130-090-851), CD15 (^{152}Sm; BioLegend, 323002), SOX2 (^{176}Yb; BD Biosciences, 561469), FOXG1 (^{145}Nd; Abcam, AbF1774), ITGA6 (^{171}Yb; R&D Systems, MAB1350), BMI1 (^{151}Eu; R&D Systems, MAB3341), and human Fab'2 (Jackson Immunoresearch, 309-545-006) were conjugated directly to the X8 chelators through a thiol linkage. In-house, synthetically raised monoclonal Fabs used for analysis were preclustered to anti-Fab'2 IgGs conjugated with X8 chelator bound with one of the following isotopes: ^{154}Sm - EPHA1, ^{169}Tm - EPHA2, ^{147}Sm - EPHA3, ^{150}Nd - EPHA4, ^{162}Dy - EPHA5, ^{173}Yb - EPHA6, ^{156}Gd - EPHA7, ^{167}Er - EPHA8, ^{160}Gd - EphA10, ^{159}Tb - EPHB1, ^{170}Er - EPHB2, ^{141}Pr - EPHB3, ^{158}Gd - EPHB4, ^{175}Lu - EPHB6. CyTOF acquisition was performed on CYTOF2 or HELIOS machine using standard settings by the UHN Flow and Mass Cytometry Facility. Acquisition was carried out on a HELIOS CyTOF system along with analysis platform, Cytobank and computational analysis software, viSNE to map the high-dimensional cytometry data for coexpression analysis.

Glioma patient database bioinformatics

To determine the clinical relevance of EphA2 and EphA3, we interrogated the REpository for Molecular Brain Neoplasia DaTa (REMBRANDT) dataset (29, 30). Expression levels were compared between gliomas (oligodendroglioma, astrocytoma, and GBM) and between GBM subtypes (proneural, classical, and mesenchymal). For survival analysis, expression levels were categorized into high and low groups for both *EPHA2* and *EPHA3* using median value as a threshold. For *EPHA2*^{high}/*EPHA3*^{high} and *EPHA2*^{low}/*EPHA3*^{low} survival analysis, expression, and patient data corresponding to *EPHA2* and *EPHA3* were obtained from The Cancer Genome Atlas (TCGA) low-grade glioma-GBM dataset (6, 29). Survival differences between the *EPHA2*^{high}/*EPHA3*^{high} (n = 193) and *EPHA2*^{low}/*EPHA3*^{low} (n = 194) groups were compared using Kaplan–Meier analysis by the log-rank test in the R "survival" package (v2.42-3). To compute differential expression between *EPHA2*^{high}/*EPHA3*^{high} and *EPHA2*^{low}/*EPHA3*^{low} groups, hg38 read count data was obtained from the NCI Genomic Data Commons Data Portal (https://portal.gdc.cancer.gov/) for the TCGA LGG and GBM datasets. The counts were merged into a single matrix, annotated with Ensembl gene annotations, and filtered to remove transcripts lacking an Entrez Gene cross-reference. In total, expression data for 374 patients (183 *EPHA2*^{high}/*EPHA3*^{high} and 191 *EPHA2*^{low}/*EPHA3*^{low}) was processed using the Bioconductor packages edgeR and Limma as follows. First, genes with less than 1 count per million (CPM) in at least 5% of the patients were filtered out, and then samples were normalized for read depth with the "calcNormFactors()" function and converted to $\log_2$ CPM with voom(). Finally, differentially expressed genes were identified using moderated t tests.

Published OnlineFirst June 26, 2018; DOI: 10.1158/0008-5472.CAN-18-0267

Sphere formation and proliferation assay

After primary sphere formation was noted, spheres were dissociated to single cells and replated in 0.2 mL Neurocult complete media as published previously (13, 31). Briefly, neurospheres were treated with Liberase Blendzyme 3 and plated at a density of 200 single cells/well for sphere formation assay and 1,000 cells/well for proliferation assay in a 96-well microwell plate in 0.2 mL volume of Neurocult complete media. The spheres were counted 3 days later. Proliferation was measured using PrestoBlue cell viability reagent (Thermo Fisher Scientific).

Lentiviral production and transduction

Lentiviral vectors expressing shRNA directed against *EPHA2* or *EPHA3* with the highest knockdown efficiency, or a control shGFP that has no targets in the human genome were used in the *in vitro* and *in vivo* experiments (sh*EPHA2*-A: 5′CCATCAAGATGCAGCAGTATA3', sh*EPHA3*-B: 5′CCTTCCAATGAAGTCAATCTA3', shGFP: 5′ACAACAGCCACAACGTCTATA3'). Both sh*EPHA2*-A and sh*EPHA3*-B were used in combination for double knockdown of *EPHA2* and *EPHA3*. Replication-incompetent lentiviruses were produced by cotransfection of the expression vector and packaging vectors pMD2G and psPAX2 in HEK 293FT cells. Viral supernatants were harvested 48 hours after transfection, filtered through a 0.45-μm cellulose acetate filter, and precipitated using ultracentrifugation (25,000 rpm, 2 hours, 4°C). The viral pellet was resuspended in 1.0 mL of Neurocult basal media and stored at −80°C. *EPHA2* shRNA and *EPHA3* shRNA with the best relative knockdown efficiencies were utilized for all *in vitro* and *in vivo* studies.

Limiting dilution assay

Cells were plated at limiting dilution from 300 cells to 1 cell per well in 200 μL of Neurocult complete media in a 96-well plate and 0.37 intercepts were calculated to determine the sphere-forming frequency (13). For *in vitro* LDA experiments, GBM cells were treated with 200 nmol/L of EphA2/A3 bispecific antibody (BsAb) or control IgG (Jacksons AffiniPure Goat Anti-Human IgG, F(ab') 2 fragment specific).

Real-time quantitative PCR

Total RNA was isolated using Norgen Total RNA Purification kit. cDNA was synthesized by iScript cDNA supermix (Quanta Biosciences) followed by real-time quantitative PCR using SsoAdvanced Universal SYBRGreenSupermix (Bio-Rad). Samples were quantified using CFX Manager software. Data are presented as the ratio of the gene of interest to GAPDH or β-actin.

Cell-cycle and apoptosis analyses

Cells were stained for DNA cell cycle using DNA Prep Reagent Kit (Beckman Coulter) and analyzed via flow cytometry (MoFlo XDP, Beckman Coulter). Annexin V conjugated to APC was used along with 7-AAD viability for analysis of apoptosis in cells of interest using flow cytometry.

RNA sequencing and analysis

Illumina sequencing was performed by the Farncombe Metagenomics Facility (McMaster University, Ontario, Canada). RNA integrity was first verified using the Agilent BioAnalyzer, followed by mRNA enrichment and library prep using the NEBNext Ultra Directional RNA Library Prep Kit along with the NEBNext Poly(A) mRNA Magnetic Isolation Module. Libraries were subject to further BioAnalyzer QC and quantified by qPCR. Sequencing was performed using the HiSeq Rapid v2 chemistry with single end 1 × 50 bp read length configurations to a target depth of approximately 6M reads per sample. Reads were aligned with the STAR v2.4.2a aligner using genome build hg38 and Gencode v25 transcript models. Read counts for each sample, output by STAR, were merged into a single matrix along with annotation information. Finally, the count matrix was filtered to only include protein-coding genes. Transcripts were removed that did not have at least 0.5 counts per million mapped reads in at least two samples, and the remaining reads were normalized using "TMM" normalization in edgeR. Differential expression was determined moderated *t* tests using Limma (v3.32.10).

Orthotopic xenografts

Animal studies were approved by and performed according to guidelines under Animal Use Protocols of McMaster University Central Animal Facility (AUP # 14-12-52). All intracranial injections were performed 2 mm anterior to the coronal suture, 3 mm lateral to midline in the right frontal lobe of 6- to 8-week-old NOD-SCID or NSG mice. rGBM BT241 cells were flow-sorted on the basis of expression of EPHA2 and EPHA3 and 6.5×10^3 cells were intracranially injected into NOD-SCID mice. A cohort of animals was sacrificed when $EPHA2^+/EPHA3^+$ engrafted mice from the experiment showed signs of tumor formation (head swelling, hunching, rough coat, weight loss) for IHC while a cohort of mice was left for survival studies. For *in vivo* LDA of $EPHA2^-/EPHA3^-$ and $EPHA2^+/EPHA3^+$ cells, 4×10^2–10^4 cells for each subpopulation of cells sorted using flow cytometry were intracranially injected into NOD-SCID mice. For EPHA2 and EPHA3 knockdown, 1×10^5 live cells of BT241 from control shGFP, sh*EPHA2*, sh*EPHA3*, and sh*EPHA2*/*A3* cells were intracranially injected into NOD-SCID mice. A cohort of animals was sacrificed 4 weeks postinjection for IHC while a cohort of mice was left for survival studies. For BT972 knockdown experiments, 6×10^5 live cells from control shGFP and *shEPHA2*/*A3* were intracranially injected NOD-SCID mice. For EPHA2/A3 BsAb treatment, 1×10^5 BT241 cells or 1×10^6 BT972 cells were intracranially injected into 6- to 8-week-old NSG mice. Intracranial treatment with EPHA2/A3 BsAb (in-house) or control IgG (Jacksons AffiniPure Goat Anti-Human IgG, F(ab')2 fragment specific) was started 10–14 days later twice a week (9.4 μL of EPHA2/A3 BsAb or control IgG for a total of 30 μg/dose) into the same burr hole created for the initial engraftment of the tumor cells. The EPHA2/A3 BsAb or control IgG were intracranially infused using a Hamilton syringe at an infusion rate of 30 μL/minute. The intracranial treatment continued for twice a week until control mice succumbed to disease burden. Mice were perfused with 10% formalin and collected brains were sliced at 2-mm thickness using brain-slicing matrix. Sections were paraffin-embedded and hematoxylin and eosin (H&E) staining and multiple IHC tests were performed (EPHA2, EPHA3, and GFAP). Tumor area was quantified using ImageJ software taking into account the scale bar measurement on the scanned H&E images.

Western blot analysis and phosphor-proteomics

For Western blotting, we used Santa Cruz Biotechnology antibodies EPHA2 (sc-924, 1:500) and EPHA3 (sc-919, 1:1,000), and Cell Signaling Technology antibodies pEPHA2 (12677S, 1:1,000), pEPHA3 (8862S, 1:1,000), ERK1/2 (4695S, 1:1,000), pERK1/2 (4377S, 1:1,000), AKT (4691S, 1:1,000), and pAKT

Published OnlineFirst June 26, 2018; DOI: 10.1158/0008-5472.CAN-18-0267

(4051S, 1:1,000). GAPDH was used as a loading control. For phosphor-proteomics, BT241 cells treated with control IgG or EPHA2/A3 BsAb (200 nmol/L for 15 minutes) were collected in urea lysis buffer (20 mmol/L HEPES, 8 mol/L urea, phosphatase inhibitor tablet – 88667, Pierce) and lysed by pipetting and sonication. After centrifugation, the lysate was treated with 1/10th of the volume of 45 mmol/L DTT (60°C, 20 minutes), cooled on ice, and then treated with 110 mmol/L iodoacetamide (room temperature in the dark, 15 minutes). Samples were diluted to a final concentration of 2 mol/L urea and treated with 1/100th of the volume of 1 mg/mL trypsin-TPCK (16 hours, dark, room temperature, rocking). Samples were treated with 1/20th the volume of 20% TFA and purified using Sep-Pak C18 columns (WAT051910, Sep-Pak). Samples were eluted in 40% acetonitrile/0.1% TFA, frozen, and lyophilized. PTMScan phosphor-tyrosine mouse mAb kit (5636, Cell Signaling Technology) was used for immunoaffinity purification. Following a 2-hour incubation at 4°C, cells were washed 5 times in IAP buffer and 3 times in water prior to elution in 0.15% TFA. Samples were concentrated and purified using C18 stage tips (87784, Pierce) and eluted in 50% acetonitrile/0.1% TFA. Samples were analyzed at the SPARC BioCentre (Hospital for Sick Children, Toronto, Ontario, Canada) by LC/MS-MS on the Q Exactive Tandem Mass Spectrometer (Thermo Fisher Scientific). Phospho-tyrosine peaks were quantified using MaxQuant (Max Planck Institute of Biochemistry, Munich, Germany) and represented as a heatmap of the intensity of the peptide in each condition over the max intensity (blue, lowest intensity; red, highest intensity).

Statistical analysis

All quantitative data presented are the mean ± SD. Samples used and respective *n* values are listed in the figure legends. The level of significance was determined by Student two-tailed *t* test or ANOVA using GraphPad Prism 5 software.

Results

EphRs are expressed heterogeneously in human GBMs and coexpress with stem cell markers

We profiled the surface protein expression of all 14 members of the EPH receptor family in primary, treatment-naïve GSCs (pGBMs: BT428, BT458, BT459, BT465, BT486, BT602 and BT648) and recurrent GSCs (rGBMs: BT241, BT566, and BT618) using our Eph profiler. The heterogeneous expression of all EphRs in human GSCs (Fig. 1A) suggests a variety of signaling paradigms that might drive oncogenesis in these patients. We observed that EPHA2 was expressed at moderate to high levels and EPHA3 was expressed at moderate levels across all GSC lines, and proceeded to characterize its expression in human neural stem and progenitor cells (NSPC), pGBMs, and rGBM by flow cytometry. Here we noted that EPHA2 and EPHA3 expression is enriched in rGBM compared with pGBM and NSPCs (Fig. 1B; Supplementary Fig. S1A). As we had previously developed a stem cell culture model of GBM recurrence (20), we treated pGBM BT602 with our *in vitro* chemoradiotherapy protocol, and noted increased expression of both *EPHA2* and *EPHA3* posttreatment (Fig. 1C). We then profiled pGBMs and rGBMs for all EphRs along with a panel of GSC markers including CD133, CD15, BMI1, SOX2, INTEGRIN-α6, and FOXG1, using mass "cytometry time-of-flight" (CyTOF) assays. CyTOF, which employs antibodies labeled with lanthanide metals rather than fluorochromes, permits a greater degree of multiplexing than traditional flow cytometry and the simultaneous quantification of numerous cell surface targets. We find that although GBMs display heterogeneous expression of these markers at the single-cell level (Fig. 1D; Supplementary Fig. S1B), there is heightened intensity of EPHA2 and EPHA3 colocalizing with GSC marker expression (Fig. 1E, population in circle). In fact, BT241, a rGBM sample, coexpressed EPHA2 and EPHA3 with all GSC markers in a population twice as large as that of two pGBMs, BT459 and BT602 (1.30% in BT241 vs. 0.52% and 0.43% in BT459 and BT602, respectively).

EPHA2 and *EPHA3* are highly expressed in GBM, overrepresented in poor-outcome subgroups of GBM, and have higher expression in rGBM

Because previous studies implicated EPHA2 and EPHA3 as independent oncogenic drivers of GSCs (24, 25), and our data suggested that EPHA2 and EPHA3 are expressed at higher levels at GBM recurrence, we interrogated *EPHA2* and *EPHA3* expression in the REMBRANDT database. Both *EPHA2* and *EPHA3* are highly expressed in GBM compared with low-grade oligodendrogliomas and astrocytomas (Fig. 2A). In addition, *EPHA2* and *EPHA3* expression was higher in classical and mesenchymal subgroups of GBM, which have a slightly worse outcome (5) when compared with the better performing proneural subgroup (Fig. 2B). In The Cancer Genome Atlas (TCGA) GBM database, we found only six matched primary-recurrent GBM pairs, and found that in a subset of these patients, the expression of *EPHA2* and *EPHA3* is higher at recurrence (Fig. 2C). High expression of *EPHA2* predicted poor survival in patients with GBM (Fig. 2D), while high expression of *EPHA3* trended toward poor but nonsignificant patients' survival (Fig. 2E). More importantly, the TCGA low-grade glioma-GBM database showed that patients with high expression of both *EPHA2* and *EPHA3* had significantly poor survival as compared with patients with low expression of both *EPHA2* and *EPHA3*, signifying that together EPHA2 and EPHA3 drive a poor prognosis in patients with gliomas (Fig. 2F). In fact, when we explored the genes associated with *EPHA2*^{high}/*EPHA3*^{high} patient subgroup, we discovered high expression of multiple genes known to promote GBM tumorigenesis such as the integrin receptors (*ITGA1*, *ITGA5*, *ITGB3*), integrin receptor ligand (*POSTN*), genes associated with tumor invasion (*CHI3L1*, *IL13RA2*, *TWIST1*, *CD70*, *IL6*), as well as genes known to mark GSCs (*PROM1*, *CA9*, *LGR6*; Fig. 2G). Together, these data led us to the hypothesis that EPHA2 and EPHA3 may coidentify an even more potent GSC population in rGBMs than expression of either EphR alone.

EPHA2 and EPHA3 coexpression marks a highly tumorigenic GSC population in rGBM

To reinforce the correlation between EPHA2 and EPHA3 coexpression in rGBM GSCs, we FACS-sorted rGBM cells into four pools, expressing either low EPHA2 and EPHA3 (EPHA2$^-$/EPHA3$^-$), high EPHA2 only (EPHA2$^+$/EPHA3$^-$), high EPHA3 only (EPHA2$^-$/EPHA3$^+$), and high EPHA2 and EPHA3 (EPHA2$^+$/EPHA3$^+$; ref. Fig. 3A), and then assessed their *in vitro* clonogenicity and intracranial tumorigenic capacity. As expected, the EPHA2$^+$/EPHA3$^+$ fraction contained the most clonogenic cells (Fig. 3B) compared with the EPHA2$^-$/EPHA3$^-$ cells, with the EPHA2$^+$/EPHA3$^-$ and EPHA2$^-$/EPHA3$^+$ cells presenting intermediate clonogenic capacity. We saw the same trend in the proliferation capacity of these fractionated cell populations (Fig. 3C). We then assessed the expression

Published OnlineFirst June 26, 2018; DOI: 10.1158/0008-5472.CAN-18-0267

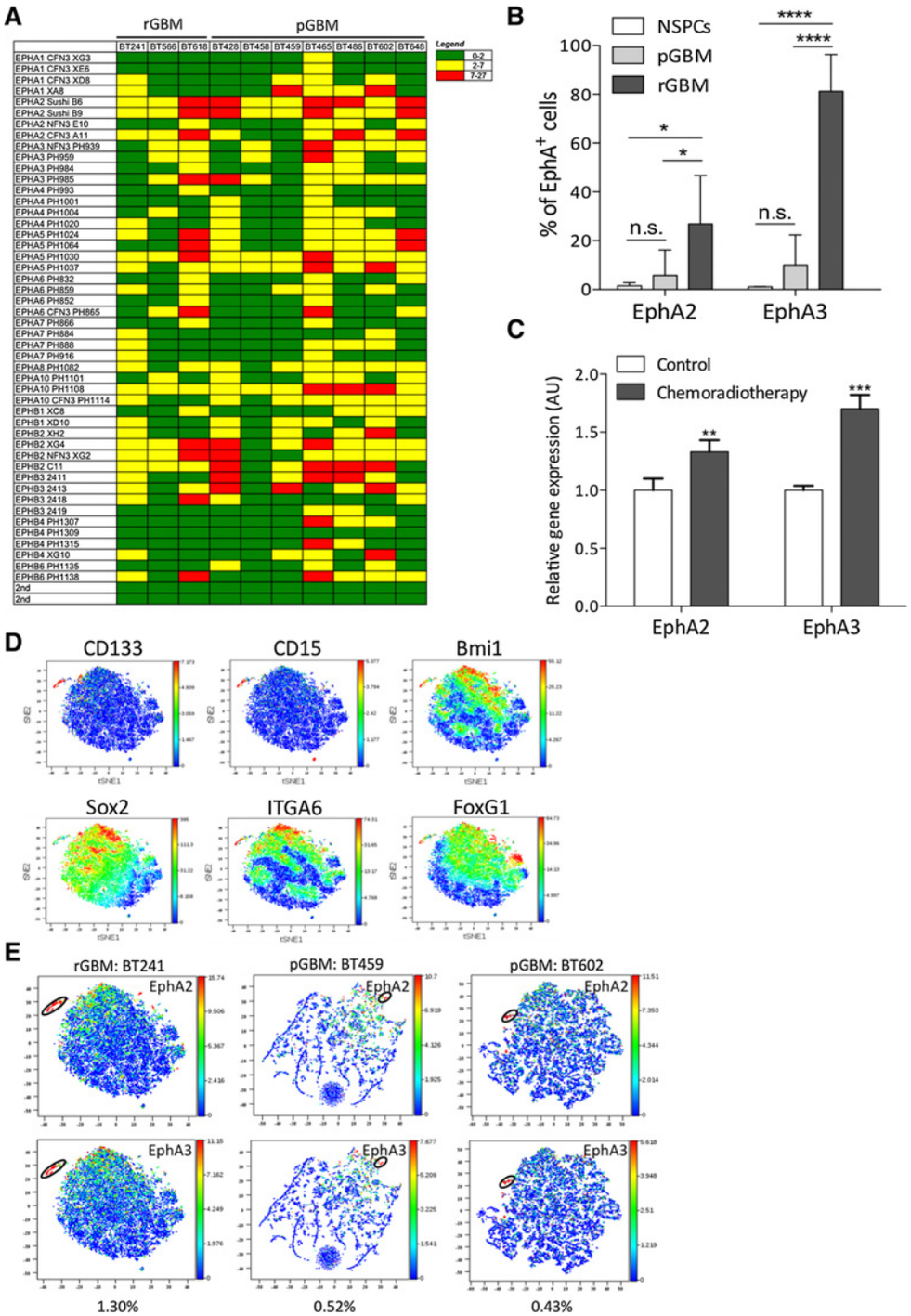

Figure 1.

EPHA2 and EPHA3 have higher expression in recurrent GBM and coexpress with GSC markers. **A,** Using the EphR profiler, we identified the expression of all 14 Eph receptors across 10 primary (BT428, BT458, BT459, BT465, BT486, BT602, BT648) and recurrent (BT241, BT566, BT618) GSC lines. **B,** Using flow cytometry, we determined the surface expression of EPHA2 and EPHA3 in human neural stem/progenitor cells (NSPC; $n = 2$), pGBM ($n = 6$), and rGBM ($n = 3$). All samples are biological replicates (EPHA2: NSPCs vs. pGBM, $P = 0.8871$; NSPCs vs. rGBM, $P = 0.0157$; pGBM vs. rGBM, $P = 0.0115$; EPHA3: NSPCs vs. pGBM, $P = 0.5542$; NSPCs vs. rGBM, $P < 0.0001$; pGBM vs. rGBM, $P < 0.0001$). **C,** pGBM (BT602) was treated with *in vitro* chemoradiotherapy and the gene expression of *EPHA2* and *EPHA3* was determined. **D,** CyTOF-based expression of GSC markers CD133, CD15, SOX2, BMI1, ITGA6, and FOXG1 in BT241. **E,** Coexpression of EPHA2 (top) and EPHA3 (bottom) with GSC markers in rGBM (BT241) and pGBMs (BT459 and BT602). The black circle represents the cellular population that coexpresses EPHA2, EPHA3, and all six GSC markers, with the percentage of cells listed at the bottom of each panel. Data are represented as mean ± SD (n.s., not significant; *, $P < 0.05$; ***, $P < 0.001$; ***, $P < 0.0001$).

Published OnlineFirst June 26, 2018; DOI: 10.1158/0008-5472.CAN-18-0267

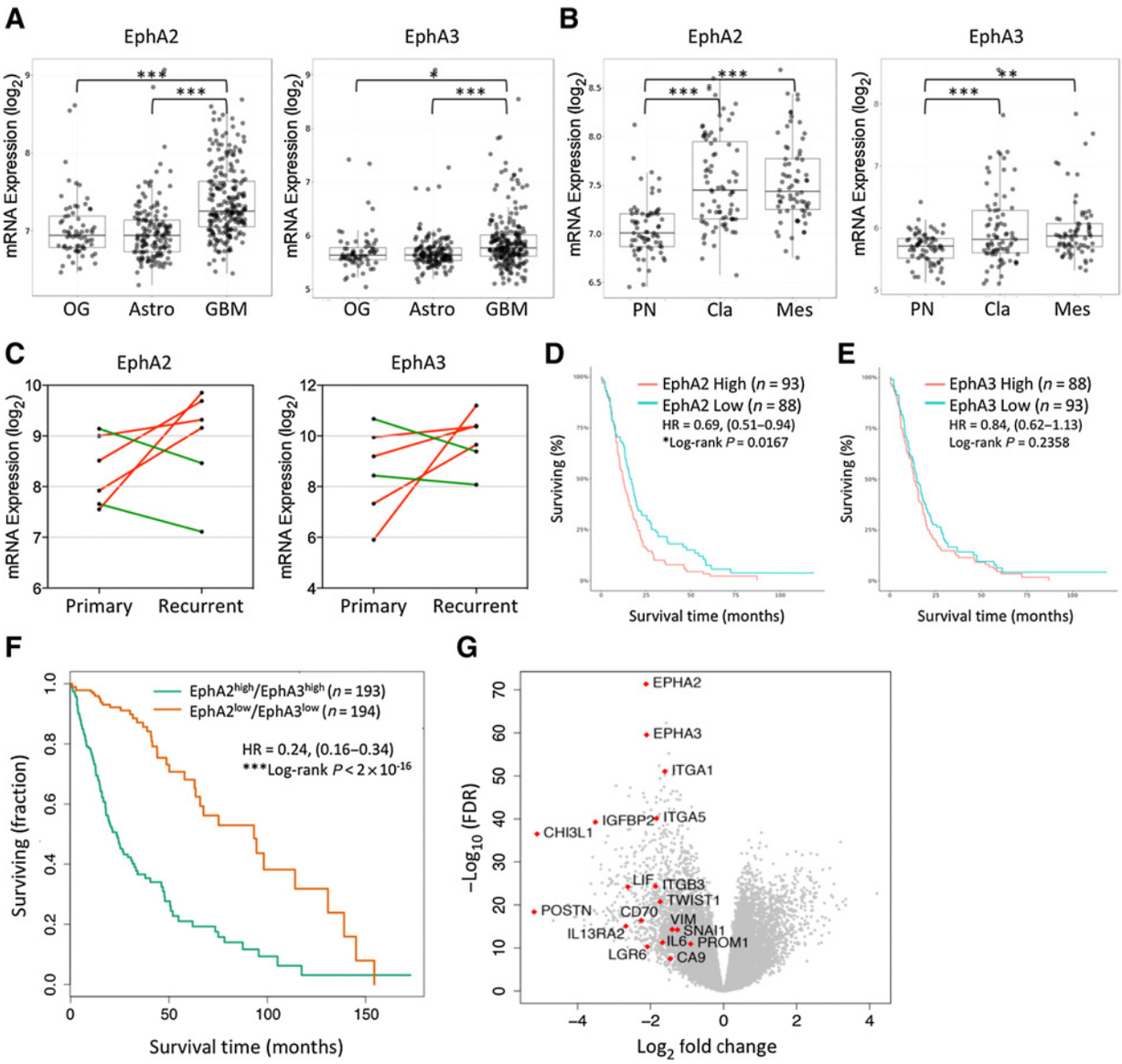

Figure 2.

High *EPHA2* and *EPHA3* coexpression correlates with poor brain tumor patient survival. **A,** *EPHA2* and *EPHA3* have higher expression in GBM (grade IV) compared with low-grade gliomas, oligodendroglioma (OG), and astrocytoma (Astro) in REMBRANDT glioma database. **B,** *EPHA2* and *EPHA3* have higher expression in classical (Cla) and mesenchymal (Mes) subgroups of GBM compared with proneural (PN) subgroup (REMBRANDT). **C,** *EPHA2* (left) and *EPHA3* (right) gene expression in paired primary GBM patient samples and their corresponding recurrent GBM tissues (TCGA, $n = 6$ matched primary-recurrent GBM tissue pairs). A subset of patients with GBM show increased expression of *EPHA2* and *EPHA3* in their recurrent tissue as compared with primary GBM. **D** and **E**, Higher expression of *EPHA2* is associated with poor survival in patients with GBM, while high expression of *EPHA3* trends toward poor but not statistically significant survival in patients with GBM (REMBRANDT). **F,** Interrogation of the TCGA low-grade glioma-GBM dataset indicates significant survival advantage for patients expressing low levels of both *EPHA2* and *EPHA3* (*EPHA2*^{low}/*EPHA3*^{low}) as compared with patients expressing high levels of both *EPHA2* and *EPHA3* (*EPHA2*^{high}/*EPHA3*^{high}). **G,** Analysis of the differentially expressed genes from patient subpopulations in **F** shows high expression of genes involved in cell invasion, epithelial–mesenchymal transition, and stemness in the *EPHA2*^{high}/*EPHA3*^{high} patient tissue (*, $P < 0.05$; **, $P < 0.01$; ***, $P < 0.001$).

of key GSC markers in EPHA2$^-$/EPHA3$^-$ and EPHA2$^+$/EPHA3$^+$ rGBM fractions and found no difference in expression of *CD133* or *CD15* but a significantly higher expression of *BMI1* and *SOX2* in EPHA2$^+$/EPHA3$^+$ cells compared with EPHA2$^-$/EPHA3$^-$ cells (Fig. 3D). Despite very low percentage of EPHA2$^+$/EPHA3$^-$ cell population and low sorting efficiency of rGBM BT241, we were able to sort cells for intracranial injections. We intracranially implanted mice with the sorted cell populations and found that EPHA2$^+$/EPHA3$^+$ cells give rise to much larger tumors compared with EPHA2$^-$/EPHA3$^-$ cells, with EPHA2$^+$/EPHA3$^-$ and EPHA2$^-$/EPHA3$^+$ cells giving rise to intermediate-sized tumors, replicating our *in vitro* clonogenic data (Fig. 3E). *In vivo* limiting dilution intracranial transplantation assays using EPHA2$^-$/EPHA3$^-$ and

Published OnlineFirst June 26, 2018; DOI: 10.1158/0008-5472.CAN-18-0267

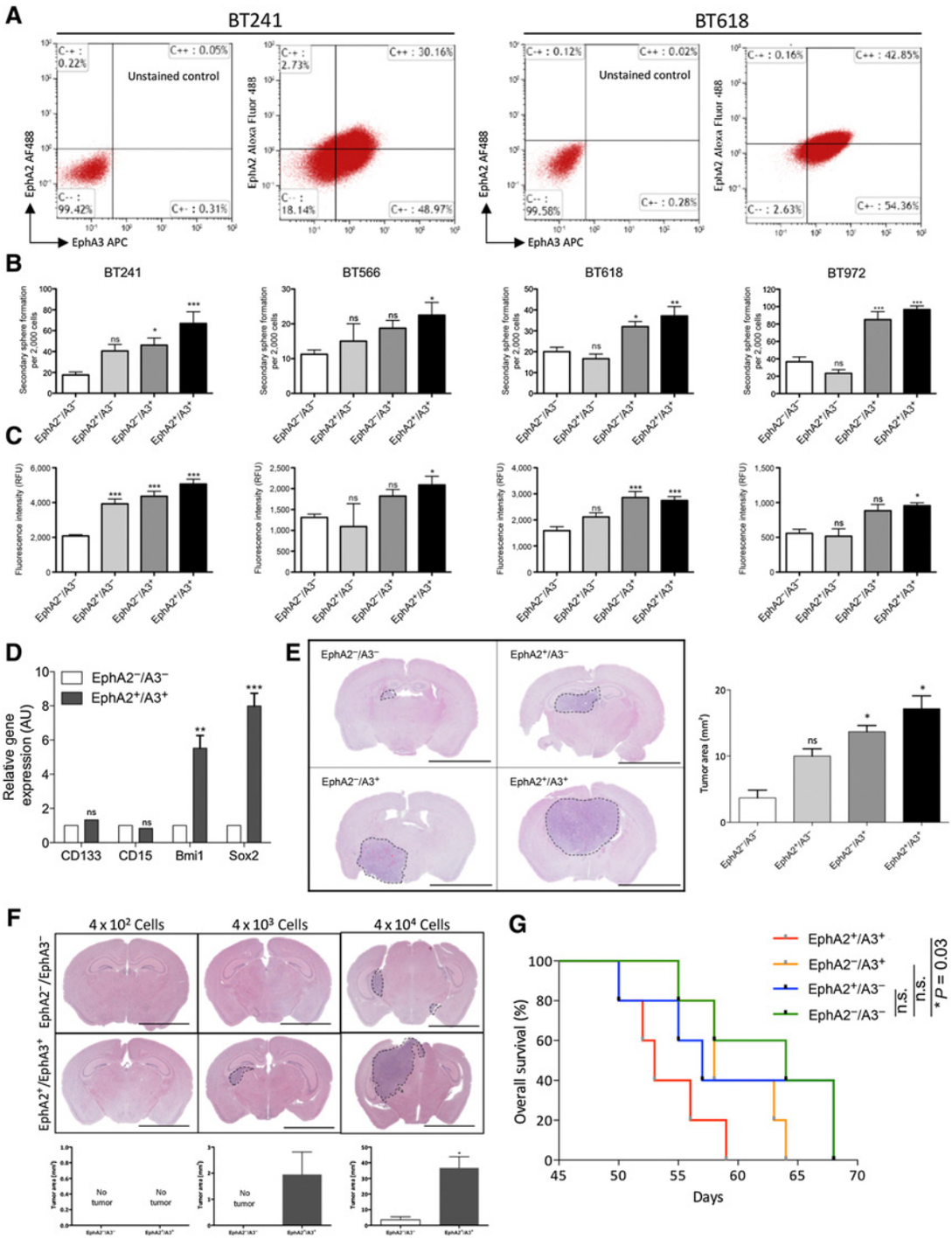

Figure 3.

Coexpression of EPHA2 and EPHA3 marks a highly clonogenic and tumorigenic cell population in recurrent GBM. **A,** Flow profile of EPHA2 and EPHA3 in two rGBM samples, BT241 and BT618. **B,** Secondary sphere formation assay of rGBMs sorted on the basis of expression of EPHA2 and EPHA3, where EPHA2$^+$/A3$^+$ exhibits the highest clonogenic capacity in four rGBMs. **C,** Proliferation assay of rGBMs sorted on the basis of the expression of EPHA2 and EPHA3, where EPHA2$^+$/EPHA3$^+$ has higher proliferation capacity than other cell populations. **D,** Gene expression of GSC markers *BMI1* and *SOX2* is higher in sorted EPHA2$^+$/EPHA3$^+$ compared with EPHA2$^-$/EPHA3$^-$ rGBM cell populations, while no difference is found in the expression of *CD133* and *CD15*. **E,** H&E staining of mice brains engrafted with rGBM BT241 cells sorted on the basis of EPHA2 and EPHA3 expression, with total tumor area presented in bar graph on the right ($n = 2$). **F,** *In vivo* limiting dilution assay of mice engrafted with different numbers of EPHA2$^-$/EPHA3$^-$ and EPHA2$^+$/EPHA3$^+$ cells, showing EPHA2$^+$/EPHA3$^+$ can form tumors at lower cell number. Bar graphs at the bottom show total tumor area of each panel ($n = 2$). **G,** Kaplan–Meier survival curves for mice engrafted with BT241 EPHA2$^-$/A3$^-$, EPHA2$^+$/A3$^-$, EPHA2$^-$/A3$^+$, EPHA2$^+$/A3$^+$ (median survival: 64, 57, 58, and 53 days, respectively; $n = 5$). Tumor area is presented in the bottom panel for each cell dose. Data are represented as mean ± SD (ns, not significant; *, $P < 0.05$; **, $P < 0.01$; ***, $P < 0.001$). Scale bar, 5 mm.

Published OnlineFirst June 26, 2018; DOI: 10.1158/0008-5472.CAN-18-0267

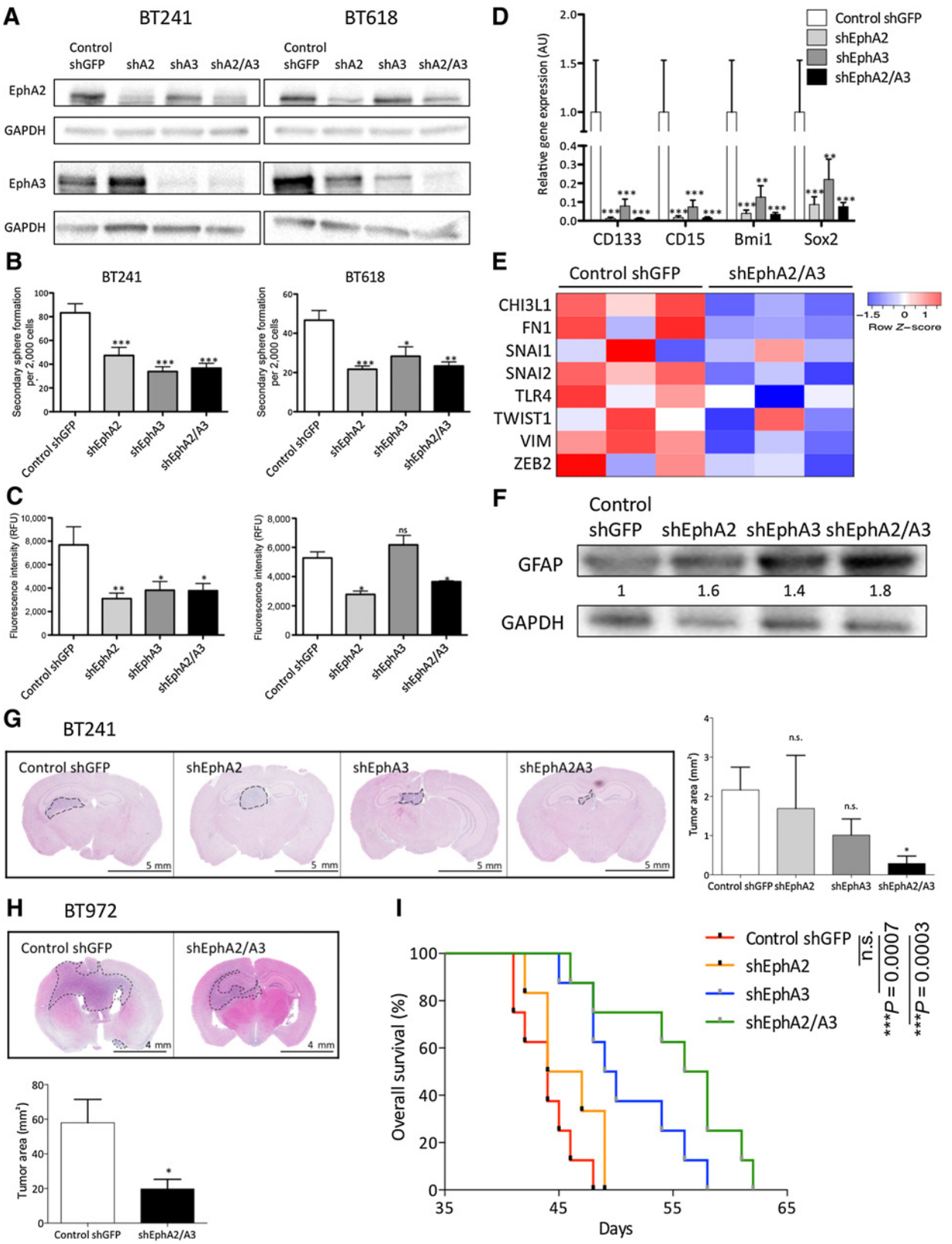

Published OnlineFirst June 26, 2018; DOI: 10.1158/0008-5472.CAN-18-0267

$EPHA2^+/EPHA3^+$ cells confirmed that high EPHA2 and EPHA3 are the hallmark GSCs in rGBM and can be used for their enrichment (Fig. 3F; stem cell frequency: $EPHA2^-/EPHA3^-$ 1/26,096 cells compared with $EPHA2^+/EPHA3^+$ 1/12,358 cells). $EPHA2^+/EPHA3^+$ cells were able to give rise to tumors with as few as 4,000 cells compared with 40,000 cells when implanting $EPHA2^-/EPHA3^-$ cells. In addition, mice engrafted with $EPHA2^+/EPHA3^+$ cells had a shorter survival (median survival 53 days) as compared with single positive cells (median survival: $EPHA2^+/EPHA3^-$ 57 days and $EPHA2^-/EPHA3^+$ 58 days) and significantly shorter than mice engrafted with $EPHA2^-/EPHA3^-$ cells (median survival 64 days, log-rank $P = 0.03$; Fig. 3G). We wanted to investigate how the cell surface expression of EPHA2 and EPHA3 in $EPHA2^+/EPHA3^+$ cells change overtime. We performed time-course experiment and found that in just four weeks, $EPHA2^+/EPHA3^+$ sorted cells revert back to their original EPHA2 and EPHA3 surface expression distribution (Supplementary Fig. S2). This suggests that the tumorigenic potential of $EPHA2^+/EPHA3^+$ would be even higher than demonstrated in *in vivo* tumor formation and survival studies as $EPHA2^+/EPHA3^+$ cells rapidly establish the original subpopulations of cells including less tumorigenic $EPHA2^+/EPHA3^-$, $EPHA2^-/EPHA3^+$, and $EPHA2^-/EPHA3^-$ cells.

Loss of EPHA2 and EPHA3 inhibits clonogenicity and tumor-forming capacity of rGBMs

We next investigated the effect of EPHA2 and EPHA3 knockdown (KD) on *in vitro* clonogenicity and intracranial tumorigenic capacity of rGBMs. We used short hairpin RNA (shRNA) to knockdown either *EPHA2* or *EPHA3* individually or in a combined fashion in two rGBM samples. We tested three separate shRNAs against *EPHA2* (sh*EPHA2*-A, B, and C) and two separate shRNAs against *EPHA3* (sh*EPHA3*-B and C), and found sh*EPHA2*-A and sh*EPHA3*-B to be the most effective at reducing protein expression of EPHA2 and EPHA3, respectively, as well as in reducing proliferation of rGBM cells (Supplementary Fig. S3A–S3D). Therefore, in all subsequent studies, we used sh*EPHA2*-A and sh*EPHA3*-B to knockdown EPHA2 and EPHA3 expression, respectively, in rGBM GSCs (Fig. 4A). We find that combined EPHA2 and EPHA3 knockdown led to loss in clonogenic capacity of rGBM cells as compared with control shGFP cells (Fig. 4B). In addition, proliferative capacity of cells was only significantly inhibited in cells with double knockdown compared with control shGFP cells (Fig. 4C). The knockdown of EPHA2 and EPHA3 also affects the cell cycle of rGBM, decreasing the percentage of cells in DNA replication S phase and increasing percentage of cells in quiescent G_0–G_1 phase (Supplementary Fig. S3E). We also noted an increase in apoptosis of rGBM with shEPHA2/A3, illustrating that EPHA2 and EPHA3 are integral to cell survival (Supplementary Fig. S3F). Furthermore, the combined EPHA2 and EPHA3 knockdown led to decreased expression of all GSC markers in rGBMs, suggesting loss of the undifferentiated, stem-like state (Fig. 4D). We next submitted control shGFP and shEPHA2/A3 cells from rGBM BT241 for RNA-sequencing for global transcriptome profiling. We found that knockdown of both EPHA2 and EPHA3 leads to reduction in gene expression of markers of epithelial–mesenchymal transition and invasion (Fig. 4E), some of which we found to be correlated with the $EPHA2^{high}/EPHA3^{high}$ patient samples (Fig. 2G), such as CHI3L1, SNAI1, and VIM. In addition, knockdown of both EPHA2 and EPHA3 increased levels of GFAP in rGBM, indicating that the decrease in EPHA2 and EPHA3 directs rGBM cells to a more differentiated, astrocytic lineage (Fig. 4F). We next intracranially implanted these cells in mice and found that combined knockdown of EPHA2 and EPHA3 completely prevented the cells from forming tumors in just under half of the transplanted mice (3/5 mice formed tumors with shEPHA2/A3 cells), while EPHA2 KD formed tumors as large as control shGFP, and EPHA3 KD formed intermediate-sized tumors (Fig. 4G). We found similar results with KD of both EPHA2 and EPHA3 in another rGBM line, BT972 (Fig. 4H). These results corroborated with survival studies where mice engrafted with shEphA2/A3 cells had the longest survival (Fig. 4I, median survival 57 days, log-rank $P = 0.0003$) as compared with control mice (median survival shGFP 44, shEPHA2 45.5 and shEPHA3 49.5 days). These results suggest that EPHA2 and EPHA3 should be cotargeted to inhibit rGBM clonogenicity, proliferation, invasion, and tumorigenic capacity potentially through a differentiation mechanism to astrocytic cell type.

Cotargeting of EPHA2 and EPHA3 with bispecific antibody decreases EPHA2 and EPHA3 surface expression and limits AKT and ERK1/2 pathway activation in rGBM

Because our data suggests that EPHA2 and EPHA3 cooperate in maintaining a potent GSC population and tumorigenic potential of rGBMs, we designed a bispecific variable heavy domain (VHD) antibody that cotargets both EPHA2 and EPHA3 (EPHA2/A3 BsAb; in-house) with high affinity (Fig. 5A and Supplementary Fig. S4A). We wanted to next determine whether binding of EPHA2/A3 BsAb leads to internalization of the BsAb. We incubated EPHA2- and EPHA3-expressing cell lines with control IgG or EPHA2/A3 BsAb at 4°C and 37°C for 4 hours (Fig. 5B; Supplementary Fig. S4B). As expected, we observed a temperature-dependent reduction of surface EPHA2/A3 BsAb binding, consistent with antibody-dependent internalization and degradation of

Figure 4.

EPHA2 and EPHA3 knockdown in rGBM inhibits clonogenicity, decreases GSC and mesenchymal marker expression, and prolongs survival. **A,** Western blot analysis showing the expression of EPHA2 and EPHA3 after shRNA-mediated knockdown (KD) of either EPHA2 or EPHA3 or both EPHA2/A3 as compared with control shGFP in two rGBMs. **B,** Secondary sphere formation assay of rGBM with knockdown against EPHA2 and EPHA3 shows decreased sphere formation capacity of shEPHA2/A3 cells. **C,** Proliferation assay of rGBMs with knockdown against EPHA2 and EPHA3 shows decreased proliferation capacity of shEPHA2/A3 cells. **D,** Gene expression of GSC markers CD133, CD15, BMI1, and SOX2 is significantly decreased in rGBMs with knockdown against EPHA2 and EPHA3. **E,** RNA sequencing results show decrease in expression of genes associated with mesenchymal and infiltrative cell type in rGBM BT241 shEPHA2/A3 cell population as compared with control shGFP cells. **F,** Western blot analysis showing the expression of GFAP after shRNA-mediated knockdown of either EPHA2 or EPHA3 or both EPHA2/A3 in rGBM BT241. **G** and **H,** H&E staining of mouse brains engrafted with rGBM BT241 control shGFP, shEPHA2, shEPHA3, or shEPHA2/A3 cells, and rGBM BT972 control shGFP or shEPHA2/A3 cells. Total tumor area is presented in the bar graph for BT241 on the right ($n = 5$, except shGFP $n = 7$) and for BT972 at the bottom ($n = 4$) of the brain images. **I,** Kaplan–Meier survival curves for mice engrafted with rGBM BT241 control shGFP, shEPHA2, shEphA3, or shEPHA2/A3 (median survival: 44, 45.5, 49.5, 57 days, respectively; $n = 8$, except shEPHA2 $n = 6$). Data are represented as mean ± SD (*, $P < 0.05$; **, $P < 0.01$; ***, $P < 0.001$).

Published OnlineFirst June 26, 2018; DOI: 10.1158/0008-5472.CAN-18-0267

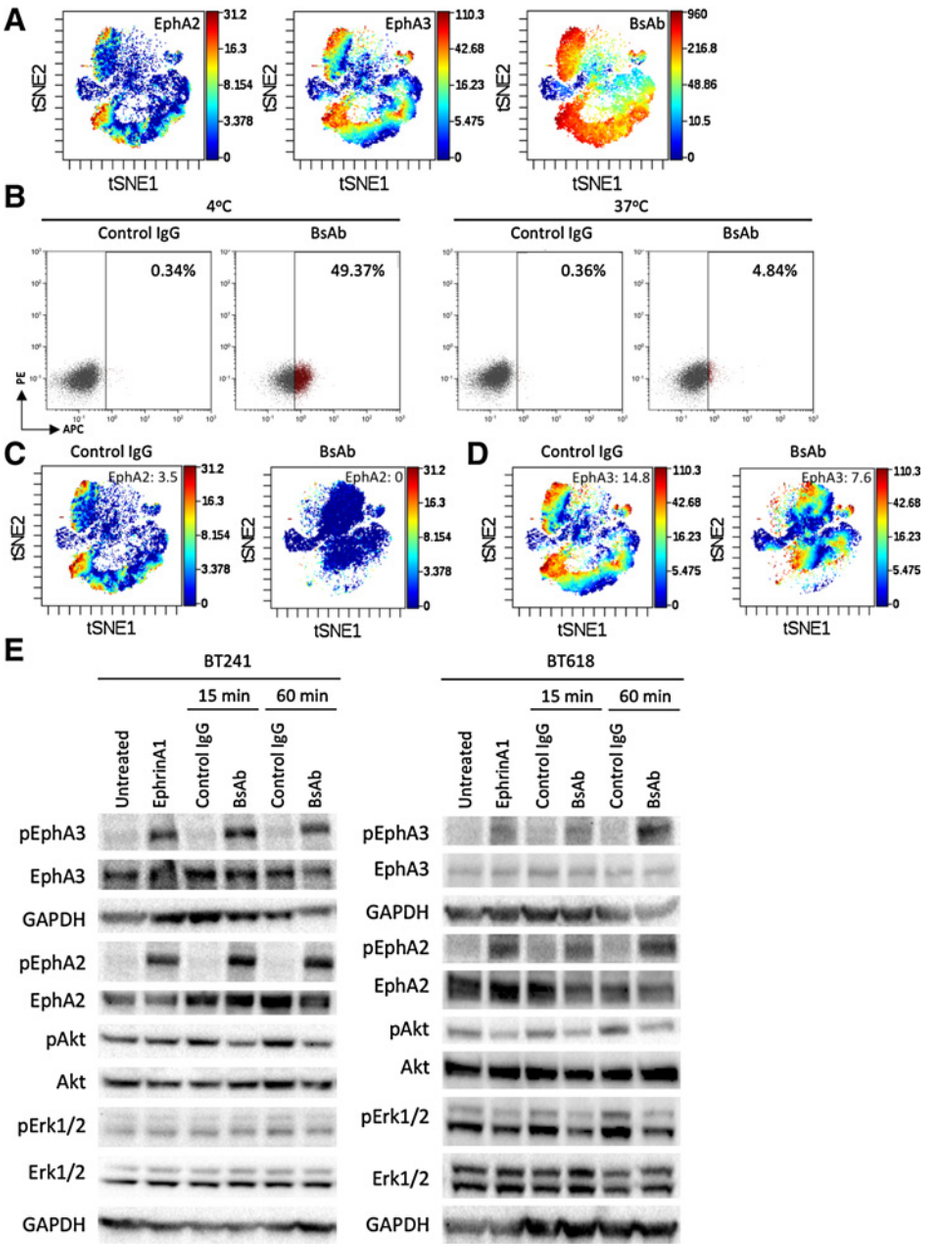

Figure 5.
Treatment of rGBM with EPHA2/A3 BsAb decreases EPHA2 and EPHA3 expression and decreases activation of AKT and ERK1/2. **A,** CyTOF analysis showing binding of BsAb to EPHA2$^+$ and EPHA3$^+$ cells in BT241. **B,** Treatment of rGBM BT241 with EPHA2/A3 BsAb at 4°C versus 37°C for 4 hours shows that the BsAb gets internalized as demonstrated by reduced BsAb binding signal at 37°C. Treatment with EPHA2/A3 BsAb for three consecutive days (200 nmol/L) decreases EPHA2 (**C**) and EPHA3 (**D**) surface expression as shown by CyTOF. Median intensity of EPHA2 and EPHA3 is shown in the top right corner of their representative plots. **E,** Western blot analysis showing protein levels of total and phosphorylated EPHA2 and EPHA3 and multiple proteins involved in downstream signaling of the EphRs when treated with EPHRINA1 ligand (15 minutes) or 200 nmol/L of control IgG or EPHA2/A3 BsAb for 15 or 60 minutes in rGBMs BT241 and BT618.

Eph receptor observed for Eph-targeting agonists. To further determine whether the internalization of the EPHA2/A3 BsAb leads to decreased surface expression of EPHA2 and EPHA3, we treated rGBM with EPHA2/A3 BsAb for three days and performed CyTOF to identify surface coexpression of EPHA2 and EPHA3. We find that treatment with EPHA2/A3 BsAb leads to a complete loss of surface EPHA2 receptor expression and an approximately 50% decrease in EPHA3 surface receptor levels (Fig. 5C and D), which was validated with Western blot analysis for total EPHA2 and EPHA3 protein levels (Supplementary Fig. S4C). After 3-day treatment with EPHA2/A3 BsAb, the EPHA2/A3 BsAb itself has much lower levels of binding to rGBM consistent with the loss of EPHA2$^+$/EPHA3$^+$ target cell population (Supplementary Fig. S4D).

We next wanted to determine the mechanism by which EPHA2/A3 BsAb reduces surface EPHA2 and EPHA3 levels. At baseline, rGBMs do not display any phosphorylation of EPHA2 or EPHA3 (Supplementary Fig. S5A; Fig. 5E, untreated lane), but it is induced in the presence of EPHRINA1 ligand (Fig. 5E). We profiled the expression of EPHRINA1 and EPHRINA5 in rGBM and found very minimal expression in our cells (Supplementary Fig. S5B). Upon further investigation, we found that EPHRINA1 and EPHRINA5, both of which activate EPHA2 and EPHA3, were highly expressed in the EPHA2$^-$/EPHA3$^-$ cell fraction as compared with the tumorigenic EPHA2$^+$/EPHA3$^+$ cells (Supplementary Fig. S5C). This possibly illustrates a bidirectional signaling mechanism between the non-GSC EPHA2$^-$/EPHA3$^-$ cells and

Published OnlineFirst June 26, 2018; DOI: 10.1158/0008-5472.CAN-18-0267

GSC EPHA2$^+$/EPHA3$^+$ cells, which coexist in a regulatory cancer stem cell niche (32).

We treated rGBM cells with EPHA2/A3 BsAb and checked for phosphorylation of EPHA2 and EPHA3 as well as known downstream targets of Eph signaling using Western blot analysis. While we saw an apparent increase in both EPHA2 and EPHA3 phosphorylation upon EPHA2/A3 BsAb treatment (Fig. 5E), given the sequence conservation of juxatmembrane pTyr sites between EPHA2 and EPHA3, we evaluated receptor phosphorylation at the peptide resolution. Indeed, phosphor-proteomics on phosphorylated tyrosines revealed high levels of phosphorylated EPHA2 peptides, but no phosphorylated EPHA3 peptides were identified, suggesting that phosphorylation induced by the EPHA2/A3 BsAb was asymmetrically driven through EPHA2 (Supplementary Fig. S5D). Consistent with this we observed decrease in EPHA2 protein levels after 60 minutes of treatment with EPHA2/A3 BsAb (Fig. 5E), whereas EPHA3 clearance was observed only after days of treatment and inequivalent to that of EPHA2 (Fig. 5D). To further explore the mechanistic regulation of EPHA2/A3 BsAb on rGBM, we assessed the activation level of downstream targets such as AKT and ERK1/2. Although 5 minutes of treatment with EphA2/A3 BsAb leads to phosphorylation of EPHA2, we found no difference in the activation of AKT and a slight decrease in activated ERK1/2 (Supplementary Fig. S5E). After 15 minutes of treatment with EPHA2/A3 BsAb, we observed a decrease in the activation of both AKT and ERK1/2 (Fig. 5E). Even after 60 minutes of treatment with EPHA2/A3 BsAb, levels of pAKT and pERK1/2 remained lower (Fig. 5E). Interestingly, *in vitro* treatment of rGBM with EPHA2/A3 BsAb does not lead to change in expression of other EphRs as shown by CyTOF profiling (Supplementary Fig. S5F), demonstrating a lack of compensatory response in an otherwise redundant EphR family signaling. Hence, treatment of rGBM with EPHA2/A3 BsAb rapidly clears the levels of EPHA2 and slowly reduces the EPHA3 receptor levels in rGBM.

EPHA2/A3 BsAb inhibits clonogenicity, promotes differentiation, and reduces tumorigenicity of rGBM

To assess the functional effects of EPHA2/A3 BsAb on rGBM, we performed secondary sphere formation and proliferation assays. Upon *in vitro* treatment of rGBMs with EPHA2/A3 BsAb, we see a reduction in both the clonogenicity (Fig. 6A and B) and proliferation capacity (Fig. 6C) of rGBMs. In fact, the activity of the EPHA2/A3 BsAb is not limited to EPHA2$^+$/EPHA3$^+$ cell fraction alone; rather the EPHA2/A3 BsAb targets EPH2$^+$/EPHA3$^-$ and EPHA2$^-$/EPHA3$^+$ cell fractions as well (Supplementary Fig. S6A and S6B), illustrating the efficacy of EPHA2/A3 BsAb against three subpopulations in rGBM. We performed an *in vitro* limiting dilution assay of rGBM cells pretreated with EPHA2/A3 BsAb and found a significant decrease in stem cell frequency of rGBM treated with EPHA2/A3 BsAb as compared with control cells (Fig. 6D; stem cell frequencies: BT241 control IgG treated 1/8 cells vs. EPHA2/A3 BsAb-treated 1/13 cells; BT618 control IgG treated 1/37 cells vs. EPHA2/A3 BsAb treated 1/78 cells; BT972 control IgG treated 1/58 cells vs. EPHA2/A3 BsAb treated 1/99 cells). To understand the mechanism of action of the EPHA2/A3 BsAb, we performed cell-cycle analysis and apoptosis assays on rGBMs treated with EPHA2/A3 BsAb as compared with control. We find that loss of clonogenicity was not caused by changes in cell cycle or apoptosis after treatment with EPHA2/A3 BsAb (Supplementary Fig. S6C and S6D). Hence, EPHA2/A3 BsAb hinders clonogenicity in rGBM GSCs independent of cell cycle and perhaps in a noncytotoxic way. To assess whether treatment with EPHA2/A3 BsAb induced a differentiation-like phenotype in rGBM, we treated rGBM with EPHA2/A3 BsAb for three consecutive days. We find that treatment with EPHA2/A3 BsAb leads to an increase in the protein levels of GFAP and MAP2, suggesting that the EPHA2/A3 BsAb acts in a similar way to EPHA2/A3 knockdown by directing rGBMs to cellular differentiation (Fig. 6E and F; Supplementary Fig. S6E).

To test the efficacy of EPHA2/A3 BsAb against rGBMs, we intracranially treated mice engrafted with rGBM (BT241 and BT972) with twice-weekly doses of 30 μg/dose of EPHA2/A3 BsAb until control mice succumbed to disease burden. Although treatment schedule had not been optimized due to limited knowledge of half-life of the EPHA2/A3 BsAb, we still found a 30%, although nonsignificant, decrease in tumor volume in mice treated with EPHA2/A3 BsAb as compared with control IgG (Fig. 6G and H) for both models of rGBM. We performed IHC on EPHA2/A3 BsAb–treated tumors to determine if any residual EPHA2$^+$ and EPHA3$^+$ population survives posttreatment. Given the EPHA2/A3 BsAb dosage limitations as described above, we saw only a slight decrease in EPHA2 and EPHA3 levels in EPHA2/A3 BsAb–treated tumors (Fig. 6I). Similar to the CyTOF results for *in vitro* treatment with EPHA2/A3 BsAb, we again see an increase in GFAP-positive cells in tumors treated with EPHA2/A3 BsAb, suggesting that the EPHA2/A3 BsAb does indeed drive the differentiation of rGBM towards the astrocytic lineage (Fig. 6J). Thus, despite intracranial dose limits, our novel EPHA2/A3 BsAb shows initial efficacy against rGBMs that are driven by EPHA2$^+$/EPHA3$^+$ GSCs.

Discussion

GBM is a lethal disease that is refractory to standard surgery and chemoradiotherapy, with the majority of patients facing tumor regrowth and uniformly fatal outcomes upon disease progression posttherapy. Intratumoral heterogeneity (ITH) at the cellular, genetic, and functional level is increasingly appreciated as a key determinant of treatment failure, and poor patient survival also correlates with increased frequency of GSCs, which are also implicated in the development of treatment resistance. Meta-analysis of recent clinical trials for patients with GBM has also predicted the failure of monotherapy to target the well-documented complexity of ITH in GBM, highlighting the need to develop innovative and informed polytherapeutic strategies for this highly complex disease.

In this article, we report the first effective application of a bispecific antibody in a preclinical, patient-derived xenograft model of recurrent GBM, thereby promoting the concept of polytargeting of multiple GSC pools that may escape therapy to drive disease recurrence. We describe the role of EPHA2 and EPHA3 receptors in cooperatively driving pathogenesis of recurrent human GBM. We report that rGBMs have enhanced expression of both EPHA2 and EPHA3 and we show that co-expression of EPHA2 and EPHA3 is directly correlated to the highly tumorigenic *in vitro* and *in vivo* capacity of these GSCs. Furthermore, loss of EPHA2 and EPHA3 expression in rGBM leads to drastic decrease in self-renewal capacity of these cells and the ability to establish intracranial rGBMs. This decrease in tumorigenicity is mediated through a loss of expression of stem cell genes and a gain in expression of differentiation markers.

Published OnlineFirst June 26, 2018; DOI: 10.1158/0008-5472.CAN-18-0267

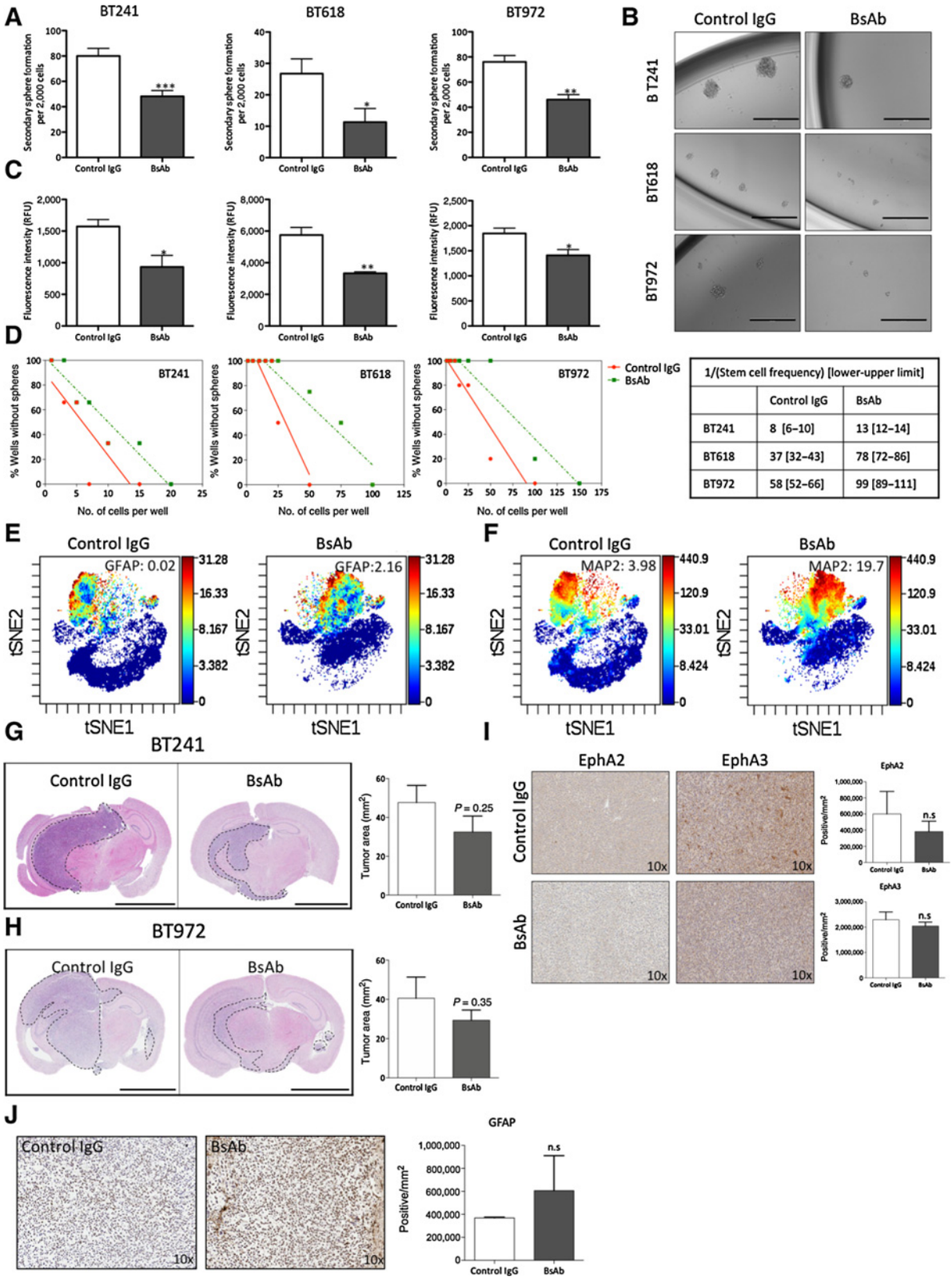

1/(Stem cell frequency) [lower-upper limit]		
	Control IgG	BsAb
BT241	8 [6–10]	13 [12–14]
BT618	37 [32–43]	78 [72–86]
BT972	58 [52–66]	99 [89–111]

Published OnlineFirst June 26, 2018; DOI: 10.1158/0008-5472.CAN-18-0267

We therefore developed a BsAb against EPHA2 and EPHA3 for targeting of this potent GSC population in rGBM. The mechanism of action of the EPHA2/A3 BsAb was mediated through phosphorylation and subsequent internalization and degradation of EPHA2 receptor and decrease in surface EPHA3 levels, which together led to the downregulation of both AKT and ERK pathways. Intracranial administration of EPHA2/A3 BsAb led to a reduction in tumor burden of established rGBMs.

Previous studies of Eph receptors in GBM had individually identified EPHA2 and subsequently EPHA3 as markers of cancer stem cells in human GBM (24, 25). However, similar to other studies in GBM, discovery of molecular targets such as EphRs has been limited to characterization in primary, *de novo* GBMs, with little focus on recurrent GBM biology. Recent studies have shown that rGBM presents a different molecular landscape, with unique clonal events driving therapy-resistant populations (12, 33). The lack of adequate models combined with limited strategies for target discovery in rGBM could explain the failure of new therapies in prolonging GBM patient survival, which are largely derived from the study of primary GBM alone. Our current investigation focused on the identification of EphRs that marked a GSC population in recurrent GBM. With the EphR profiler, we elucidated the differential expression of all 14 EphR in recurrent and primary GSC lines. We then found that EPHA2 and EPHA3 were enriched in rGBM. Further characterization of EphR expression in GBM using CyTOF showed that EPHA2 and EPHA3 coexpressed with multiple known GSC markers, and that this coexpression was enhanced in rGBM, possibly identifying EPHA2/A3 coexpressing cells as a stem-cell like population in rGBM. Upon analyzing a large GBM dataset (REMBRANDT), we identified high expression of EPHA2 and EPHA3 as being characteristic of the poor-performing classical and mesenchymal subgroups of GBM and also predicted lower survival in GBM. Importantly, despite the few recurrent GBM samples present in the TCGA dataset, we identified trends of higher expression of EPHA2 and EPHA3 in recurrent GBM as compared with primary GBM. Altogether, this illustrated that EPHA2 and EPHA3 together may mark a tumorigenic GSC population exclusive to recurrent GBM.

Conclusive evidence of the idea that coexpression of EPHA2 and EPHA3 marked a rGBM GSC population came from fractionating rGBM into $EPHA2^-/EPHA3^-$, $EPHA2^+/EPHA3^-$, $EPHA2^-/EPHA3^+$ and $EPHA2^+/EPHA3^+$ populations. The highest *in vitro* clonogenic potential and *in vivo* tumorigenic potential was associated with combined high EPHA2/EPHA3 expression ($EPHA2^+/EPHA3^+$). The EPHA2/EPHA3 coexpressing population also had the highest expression of known GSC markers, BMI1 and SOX2, validating our CyTOF data. The fact that cell population that coexpresses both EPHA2 and EPHA3 may drive rGBM GSC was reinforced by the fact that knockdown of both EPHA2 and EPHA3 was required to significantly reduce *in vitro* tumorigenicity of rGBM. In fact, intracranial injection of rGBM with double EPHA2/EPHA3 knockdown abrogated tumor initiation in almost half of the mice, while single EPHA2 or EPHA3 knockdown still led to initiation of tumors in all mice. In addition, knockdown of both EPHA2 and EPHA3 led to a significant increase in astrocytic differentiation marker GFAP, suggesting the decrease in tumorigenicity is driven by an increase in differentiation of GBM cells. For the first time, we show that two EphR together mark and drive a highly potent GSC population in recurrent GBM, where loss of EPHA2 and EPHA3 together promotes differentiation of GBM.

Considering that GBM presents with extensive ITH, it is no surprise that we identified multiple GSC populations cooperating in driving tumorigenesis of GBM. Despite that, new therapies continue to focus on single targets and rely on monotherapies to promote patient survival. As multiple cellular populations promote tumorigenic phenotype, single population targeting by monotherapies allows other cellular populations to escape therapy and seed disease recurrence. Our work aims to change that paradigm by presenting evidence of multiple GSC pools in recurrent GBM that may be cotargeted for improved patient outcome. Other ephrin poly-targeting strategies have been described in GBM, notably an EPHA2, A3, and B2-targeting agent composed of EPHRINA5 ligand linked to a cytotoxin that demonstrated efficacious cell killing *in vitro* (34). This ligand-based polytargeting strategy is however limited by a lack of target specificity, as ephrin ligands can be expected to bind a multitude of EphRs in many cells and tissues, such that off-target effects and resultant *in vivo* toxicity are likely. We proposed a more precise poly-targeting strategy through the development of a bispecific antibody against both EPHA2 and EPHA3 driven GSC population in recurrent GBM. The treatment of rGBM with EPHA2/A3 BsAb reduced clonogencity and proliferative capacity of the cells, mediated through a reduction in EPHA2 and EPHA3 levels, which in turn downregulated AKT and ERK1/2, known oncogenic pathways in GBM. The attenuation of EPHA2 and EPHA3 by EPHA2/A3 BsAb also resulted in partial differentiation as evidenced by an increase in GFAP and MAP2 levels, mimicking the effect of knockdown of these receptors.

Although we had limited knowledge of the pharmacokinetics and pharmacodynamics of the EPHA2/A3 BsAb, we tested the efficacy of EPHA2/A3 BsAb in reducing established recurrent GBM xenografts through twice-weekly intracranial doses of the EPHA2/A3 BsAb and noted a reduction in tumor growth, a decrease in EPHA2 and EPHA3 expression, and an increase in GFAP levels. In addition, studies by Brown and colleagues have shown that

Figure 6.

Treatment of rGBM with EPHA2/A3 BsAb inhibits *in vitro* clonogenicity, increases differentiation, and reduces tumor burden. **A,** Secondary sphere formation assay of rGBM treated with 200 nmol/L EPHA2/A3 BsAb shows a decrease in clonogenic capacity as compared with control IgG–treated cells. **B,** rGBM treated with 200 nmol/L EPHA2/A3 BsAb have fewer and smaller spheres (scale bar, 400 μm). **C,** Proliferation assay of rGBMs treated with EPHA2/A3 BsAb shows decreased proliferation compared with control IgG–treated cells. **D,** Limiting dilution assay of rGBM pretreated with 200 nmol/L of EPHA2/A3 BsAb for 3 days. The table on the right shows the stem cell frequencies and upper and lower limits. Protein expression of GFAP (**E**) and MAP2 (**F**) using CyTOF in BT241 after 3-day treatment with 200 nmol/L of EPHA2/A3 BsAb. The number in the top right corner of each plot represents median intensity. **G** and **H,** H&E staining of mouse brains engrafted with rGBMs BT241 or BT972, treated with 30 μg intracranial biweekly dose of control IgG or EPHA2/A3 BsAb, until control mice succumbed to disease burden. Total tumor area is presented in the bar graphs on the right of each IHC panel (BT241, $n = 6$; BT972, $n = 5$). **I,** EPHA2 (left) and EPHA3 (right) staining on BT241, control IgG, or EPHA2/A3 BsAb–treated tumors. Bar graphs on the right represents average positive staining per mm^2 of tumor area for both EPHA2 and EPHA3 ($n = 3$). **J,** GFAP staining on BT241, control IgG, or EPHA2/A3 BsAb-treated tumors. Bar graph on the right represents average positive staining per mm^2 of tumor area. Data are represented as mean ± SD (n.s., not significant; *, $P < 0.05$; **, $P < 0.01$; ***, $P < 0.001$). Scale bar on IHC images represent 4 mm.

Published OnlineFirst June 26, 2018; DOI: 10.1158/0008-5472.CAN-18-0267

intracranial delivery of therapy for patients with GBM is safe and well tolerated (35), with intraventricular infusion showing greater efficacy against multinodal, infiltrative tumors as compared with intracavitary infusion (36, 37). This demonstrates that our current intracranial therapy delivery model of the BsAb will be a viable option for patients with recurrent GBM. Critical to our approach was the development and validation of autonomous VHD capable of selectively targeting and modulating GBM-specific tumor antigens with high affinity. While mass transport of VHD-Fc through the BBB is unlikely in its current format, the size (~13 kDa) and single-chain format of the VHD is ideal for the engineering of fusion proteins that enable mass transport (38–40). Optimization of the modality for systemic delivery, biodistribution, and therapeutic efficacy remain important goals for further therapeutic development. The EPHA2/A3 BsAb hence dually targets a highly tumorigenic, multitarget-driven GSC population in recurrent GBM through the promotion of a differentiation phenotype. The mechanism of action of the BsAb is through phosphorylation and internalization of the EPHA2 receptor, leading to its degradation, whereas the decrease in EPHA3 at the cell surface appears to be phosphorylation-independent. The latter finding is not surprising, as anti-EPHA3 antibodies in clinical trials for advanced hematologic malignancies induce reduction of EPHA3 levels and subsequent apoptosis and activation of antibody-dependent cell-mediated cytotoxicity in treated leukemia cells, with no evidence of phosphorylation of EPHA3; thus the mechanism of EPHA3 receptor reduction at the cell surface remains unknown (41). Future optimization of the EPHA3-depleting features of our EPHA2/A3 BsAb by exploring unique epitopes or valencies could perhaps further enhance the reduction of tumor burden, to the degree observed in our knockdown studies.

Therapeutic mAbs have several major limitations in their mode of action, including redundancy of molecular pathways leading to tumor cell survival, effects of the microenvironment, and activation of inhibitory receptors. To overcome the functional redundancy among pro-tumorigenic signaling pathways we empirically applied a BsAb modality to target heterogeneous GSC populations, while also blocking the activity of the protumorigenic non-GSC populations that comprise the tumor niche. Comprehensive profiling of the entire EphR family in recurrent human GBM and in-depth functional characterization of GSC populations that contribute to ITH have together generated a novel, empiric poly-targeted therapy that offers a new and promising treatment paradigm for patients with recurrent GBM.

Disclosure of Potential Conflicts of Interest

No potential conflicts of interest were disclosed.

Authors' Contributions

Conception and design: M.A. Qazi, P. Vora, C. Venugopal, J. Adams, J. Moffat, S. Sidhu, S.K. Singh

Development of methodology: M.A. Qazi, P. Vora, J. Adams, S.K. Singh

Acquisition of data (provided animals, acquired and managed patients, provided facilities, etc.): M.A. Qazi, P. Vora, M. Singh, A.X. Hu, M. Gorelik, M.K. Subapanditha, N. Savage, C. Chokshi, M. London, A. Gont, D. Bobrowski, N. Grinshtein, N.K. Murty, J. Nilvebrant, S.K. Singh

Analysis and interpretation of data (e.g., statistical analysis, biostatistics, computational analysis): M.A. Qazi, P. Vora, J. Adams, M. Singh, A.X. Hu, M. Gorelik, M.K. Subapanditha, N. Savage, J. Yang, C. Chokshi, M. London, A. Gont, D. Bobrowski, N. Grinshtein, K.R. Brown, J. Nilvebrant, D.R. Kaplan, S. Sidhu, S.K. Singh

Writing, review, and/or revision of the manuscript: M.A. Qazi, P. Vora, C. Venugopal, J. Adams, M. Singh, A.X. Hu, M. Gorelik, M.K Subapanditha, N. Savage, C. Chokshi, M. London, A. Gont, D. Bobrowski, K.R. Brown, J. Nilvebrant, D.R. Kaplan, J. Moffat, S. Sidhu, S.K. Singh

Administrative, technical, or material support (i.e., reporting or organizing data, constructing databases): P. Vora, N.K. Murty

Study supervision: S.K. Singh

Acknowledgments

M.A. Qazi is supported by the Canadian Institute of Health Research Canada Graduate Scholarship - Doctoral. This study was funded by Terry Fox Research Institute Program Project Grant awarded to J. Mofatt, S. Sidhu, and S.K. Singh. We thank Mr. Mohammad Ali Malik for assisting with animal work and assembly of data.

The costs of publication of this article were defrayed in part by the payment of page charges. This article must therefore be hereby marked *advertisement* in accordance with 18 U.S.C. Section 1734 solely to indicate this fact.

Received January 25, 2018; revised May 14, 2018; accepted June 22, 2018; published first June 26, 2018.

References

1. Louis DN, Ohgaki H, Wiestler OD, Cavenee WK, Burger PC, Jouvet A, et al. The 2007 WHO classification of tumours of the central nervous system. Acta Neuropathol 2007;114:97–109.
2. Louis DN, Perry A, Reifenberger G, Deimling von A, Figarella-Branger D, Cavenee WK, et al. The 2016 World Health Organization Classification of Tumors of the Central Nervous System: a summary. Acta Neuropathol 2016;131:803–20.
3. Stupp R, Hegi ME, Mason WP, van den Bent MJ, Taphoorn MJ, Janzer RC, et al. Effects of radiotherapy with concomitant and adjuvant temozolomide versus radiotherapy alone on survival in GBM in a randomised phase III study: 5-year analysis of the EORTC-NCIC trial. Lancet Oncol 2009; 10:459–66.
4. Stupp R, Taillibert S, Kanner A, Read W, Steinberg D, Lhermitte B, et al. Effect of tumor-treating fields plus maintenance Temozolomide vs maintenance Temozolomide alone on survival in patients with GBM: a randomized clinical trial. JAMA 2017;318:2306–16.
5. Verhaak RGW, Hoadley KA, Purdom E, Wang V, Qi Y, Wilkerson MD, et al. Integrated genomic analysis identifies clinically relevant subtypes of GBM characterized by abnormalities in PDGFRA, IDH1, EGFR, and NF1. Cancer Cell 2010;17:98–110.
6. Brennan CW, Verhaak RGW, McKenna A, Campos B, Noushmehr H, Salama SR, et al. The somatic genomic landscape of GBM. Cell 2013; 155:462–77.
7. McLendon R, Friedman A, Bigner D, Van Meir EG, Brat DJ, M Mastrogianakis G, et al. Comprehensive genomic characterization defines human GBM genes and core pathways. Nature 2008;455: 1061–8.
8. Patel AP, Tirosh I, Trombetta JJ, Shalek AK, Gillespie SM, Wakimoto H, et al. Single-cell RNA-seq highlights intratumoral heterogeneity in primary GBM. Science 2014;344:1396–401.
9. Meyer M, Reimand J, Lan X, Head R, Zhu X, Kushida M, et al. Single cell-derived clonal analysis of human glioblastoma links functional and genomic heterogeneity. Proc Natl Acad Sci USA 2015;112:851–6.
10. Kim J, Lee I-H, Cho HJ, Park C-K, Jung Y-S, Kim Y, et al. Spatiotemporal evolution of the primary GBM genome. Cancer Cell 2015;28:318–28.
11. Johnson BE, Mazor T, Hong C, Barnes M, Aihara K, McLean CY, et al. Mutational analysis reveals the origin and therapy-driven evolution of recurrent glioma. Science. 2014;343:189–93.
12. Wang J, Cazzato E, Ladewig E, Frattini V, Rosenbloom DIS, Zairis S, et al. Clonal evolution of GBM under therapy. Nat Genet 2016;48:768–76.

Published OnlineFirst June 26, 2018; DOI: 10.1158/0008-5472.CAN-18-0267

13. Singh SK, Clarke ID, Terasaki M, Bonn VE, Hawkins C, Squire J, et al. Identification of a cancer stem cell in human brain tumors. Cancer Res 2003;63:5821–8.
14. Son MJ, Woolard K, Nam D-H, Lee J, Fine HA. SSEA-1 is an enrichment marker for tumor-initiating cells in human GBM. Cell Stem Cell 2009;4:440–52.
15. Lathia JD, Gallagher J, Heddleston JM, Wang J, Eyler CE, Macswords J, et al. Integrin alpha 6 regulates GBM stem cells. Cell Stem Cell 2010;6:421–32.
16. Suva ML, Rheinbay E, Gillespie SM, Patel AP, Wakimoto H, Rabkin SD, et al. Reconstructing and reprogramming the tumor-propagating potential of GBM stem-like cells. Cell 2014;157:580–94.
17. Bao S, Wu Q, McLendon RE, Hao Y, Shi Q, Hjelmeland AB, et al. Glioma stem cells promote radioresistance by preferential activation of the DNA damage response. Nature 2006;444:756–60.
18. Liu G, Yuan X, Zeng Z, Tunici P, Ng H, Abdulkadir IR, et al. Analysis of gene expression and chemoresistance of CD133+ cancer stem cells in GBM. Mol Cancer 2006;5:67.
19. Chen J, Li Y, Yu T-S, McKay RM, Burns DK, Kernie SG, et al. A restricted cell population propagates GBM growth after chemotherapy. Nature 2012;488:1–6.
20. Qazi MA, Vora P, Venugopal C, McFarlane N, Subapanditha MK, Murty NK, et al. A novel stem cell culture model of recurrent GBM. J Neurooncol 2016;126:57–67.
21. Pasquale EB. Eph-Ephrin bidirectional signaling in physiology and disease. Cell 2008;133:38–52.
22. Genander M, Frisén J. Ephrins and Eph receptors in stem cells and cancer. Curr Opin Cell Biol 2010;22:611–6.
23. Nakada M, Hayashi Y, Hamada JI. Role of Eph/ephrin tyrosine kinase in malignant glioma. Neuro Oncol 2011;13:1163–70.
24. Binda E, Visioli A, Giani F, Lamorte G, Copetti M, Pitter KL, et al. The EphA2 receptor drives self-renewal and tumorigenicity in stem-like tumor-propagating cells from human GBMs. Cancer Cell 2012;22:765–80.
25. Day BW, Stringer BW, Al-Ejeh F, Ting MJ, Wilson J, Ensbey KS, et al. EphA3 maintains tumorigenicity and is a therapeutic target in glioblastoma multiforme. Cancer Cell. 2013;23:238–48.
26. Nakada M, Anderson EM, Demuth T, Nakada S, Reavie LB, Drake KL, et al. The phosphorylation of ephrin-B2 ligand promotes glioma cell migration and invasion. Int J Cancer 2009;:NA–NA.
27. Wykosky J. EphA2 as a novel molecular marker and target in GBM multiforme. Mol Cancer Res 2005;3:541–51.
28. Miao H, Gale NW, Guo H, Qian J, Petty A, Kaspar J, et al. EphA2 promotes infiltrative invasion of glioma stem cells in vivo through cross-talk with Akt and regulates stem cell properties. Oncogene 2014;34:558–67
29. Bowman RL, Wang Q, Carro A, Verhaak RGW, Squatrito M. GlioVis data portal for visualization and analysis of brain tumor expression datasets. Neuro Oncol 2017;19:139–41.
30. Madhavan S, Zenklusen J-C, Kotliarov Y, Sahni H, Fine HA, Buetow K. Rembrandt: helping personalized medicine become a reality through integrative translational research. Mol Cancer Res 2009;7:157–67.
31. Singh SK, Hawkins C, Clarke ID, Squire JA, Bayani J, Hide T, et al. Identification of human brain tumour initiating cells. Nature 2004;432:396–401.
32. Plaks V, Kong N, Werb Z. The cancer stem cell niche: how essential is the niche in regulating stemness of tumor cells? Cell Stem Cell2015;16:225–38.
33. Kim H, Zheng S, Amini SS, Virk SM, Mikkelsen T, Brat DJ, et al. Whole-genome and multisector exome sequencing of primary and post-treatment GBM reveals patterns of tumor evolution. Genome Res 2015;25:316–27.
34. Ferluga S, Tomé CML, Herpai DM, D'Agostino R, Debinski W. Simultaneous targeting of Eph receptors in GBM. Oncotarget 2016;7:59860–76.
35. Brown CE, Badie B, Barish ME, Weng L, Ostberg JR, Chang W-C, et al. Bioactivity and safety of IL13Rα2-redirected chimeric antigen receptor CD8+ T cells in patients with recurrent glioblastoma. Clin Cancer Res 2015;21:4062–72.
36. Brown CE, Alizadeh D, Starr R, Weng L, Wagner JR, Naranjo A, et al. Regression of GBM after chimeric antigen receptor T-cell therapy. N Engl J Med 2016;375:2561–9.
37. Priceman SJ, Tilakawardane D, Jeang B, Murad JP, Park AK, Chang W-C, et al. Regional delivery of chimeric antigen receptor-engineered T Cells effectively targets HER2+ breast cancer metastasis to the brain. Clin Cancer Res 2017;24:95–105.
38. Dufès C, Robaian Al M, Somani S. Transferrin and the transferrin receptor for the targeted delivery of therapeutic agents to the brain and cancer cells. Ther Deliv 2013;4:629–40.
39. Nikanjam M, Blakely EA, Bjornstad KA, Shu X, Budinger TF, Forte TM. Synthetic nano-low density lipoprotein as targeted drug delivery vehicle for GBM multiforme. Int J Pharm 2007;328:86–94.
40. Zhang B, Sun X, Mei H, Wang Y, Liao Z, Biomaterials JC, et al. LDLR-mediated peptide-22-conjugated nanoparticles for dual-targeting therapy of brain glioma. Biomaterials 2013;34:9171–82.
41. Swords RT, Greenberg PL, Wei AH, Durrant S, Advani AS, Hertzberg MS, et al. KB004, a first in class monoclonal antibody targeting the receptor tyrosine kinase EphA3, in patients with advanced hematologic malignancies: Results from a phase 1 study. Leuk Res 2016;50:123–31.

Published OnlineFirst June 26, 2018; DOI: 10.1158/0008-5472.CAN-18-0267

Cancer Research
The Journal of Cancer Research (1916–1930) | The American Journal of Cancer (1931–1940)

AACR American Association for Cancer Research

Cotargeting Ephrin Receptor Tyrosine Kinases A2 and A3 in Cancer Stem Cells Reduces Growth of Recurrent Glioblastoma

Maleeha A. Qazi, Parvez Vora, Chitra Venugopal, et al.

Cancer Res 2018;78:5023-5037. Published OnlineFirst June 26, 2018.